Letter

Universal spin-mixing oscillations in a strongly interacting one-dimensional Fermi gas

Giovanni Pecci,[1] Patrizia Vignolo,[2] and Anna Minguzzi[1]
[1]*Université Grenoble Alpes, CNRS, LPMMC, 38000 Grenoble, France*
[2]*Université Côte d'Azur, CNRS, Institut de Physique de Nice, 06560 Valbonne, France*

(Received 26 July 2021; revised 6 April 2022; accepted 10 May 2022; published 31 May 2022)

We study the spin-mixing dynamics of a one-dimensional strongly repulsive Fermi gas under harmonic confinement. By employing a mapping onto an inhomogeneous isotropic Heisenberg model and the symmetries under particle exchange, we follow the dynamics until very long times. Starting from an initial spin-separated state, we observe superdiffusion, spin-dipolar large amplitude oscillations, and thermalization. We report a universal scaling of the oscillations with particle number $N^{1/4}$. Our Letter puts forward one-dimensional correlated fermions as a different system to observe the emergence of nonequilibrium universal features.

DOI: 10.1103/PhysRevA.105.L051303

I. INTRODUCTION

Elucidating the dynamics of interacting Fermi gases is important for understanding a large variety of physical phenomena, from condensed matter to plasmas and astrophysical objects as neutron stars. The strongly out-of-equilibrium dynamics of interacting quantum systems is currently one of the most challenging open problems.

In this context, the spin dynamics deserves a specific focus. Spin currents can be easily damped by interparticle collisions [1] and the continuity equation for the spin density includes both orbital current and spin torque contributions [2]. Spin drag is another manifestation of interactions among the spin species, inducing spin-diffusive or nondissipative dynamics depending on the interaction regimes [1,3–7]. Ultracold atomic gases provide an ideal platform for exploring in isolated conditions the out-of-equilibrium spin dynamics [8–10]. In a three-dimensional geometry, the oscillatory dynamics of a strongly interacting Fermi gas with initially spatially separated spin components was studied in Ref. [11]. The spin drag, spin diffusivity, and spin susceptibility were obtained, and a universal limit for spin diffusivity at low temperature was reported for the unitary Fermi gas.

A relevant question is what happens to the above quantities when reducing the dimensionality of the system to quasi-one-dimensional (1D), and what type of universality emerges. One-dimensional systems display specific features, as the enhancement of quantum fluctuations and correlations, and they can be described by a wealth of theoretical and numerical methods [12–15]. The quantum dynamics may be strongly affected by the geometrical constraints, as well as by the presence of a large number of conserved quantities, as demonstrated, e.g., in the quantum Newton cradle experiment [16].

We address this question by following the dynamics of strongly repulsive fermions subjected to a longitudinal harmonic confinement in a tight waveguide. As in the three-dimensional case of Ref. [11], we start from an initially imbalanced state with all spin up on the left and all spin down on the right of the harmonic trap, and we follow the damped oscillations of the magnetization. While the fully quantum dynamics at arbitrary interactions can be followed only at short times with a classical simulator, we focus here on the strongly correlated regime of very large interactions, close to the integrable point at infinite repulsions [17–23]. In this regime, the dynamics of the charge and spin decouple, and the spin dynamics can be followed exactly until very long times by means of a mapping onto the one of an inhomogeneous, isotropic Heisenberg model [24,25] with site-dependent couplings [26,27].

An overview of the full spin dynamics is provided in Fig. 1, where three main dynamical regimes arise. At short times, we predict the emergence of a superdiffusive behavior, compatible with Kardar-Parisi-Zhang (KPZ) universality, in striking difference from the diffusive one found in the three-dimensional counterpart [11]. We thus identify 1D correlated fermions as a different system to observe the emergence of nonequilibrium universality, largely explored in homogeneous Heisenberg models [28–35] and experimentally evidenced in quantum magnets and in ultracold atoms on a lattice [36–39]. At intermediate times, we observe large-amplitude spin-dipole oscillations and we obtain the spin drag decay rate. We unveil a $N^{1/4}$ scaling in the oscillation frequency, implying a slowdown of the motion and the decrease of the zero-temperature spin drag rate as the particle number grows.

At long times, the oscillations are damped out and the system thermalizes to the diagonal ensemble [40]. From the analysis of the energy levels' distribution we find that the system is weakly nonintegrable. The proposed setup allows us to explore the conditions for emergence of nonequilibrium universal behavior in relation to the breaking of its integrability in one dimension.

II. MODEL AND DYNAMICS

We consider a one-dimensional $SU(2)$ interacting Fermi gas confined in a harmonic trap. The Hamiltonian for such

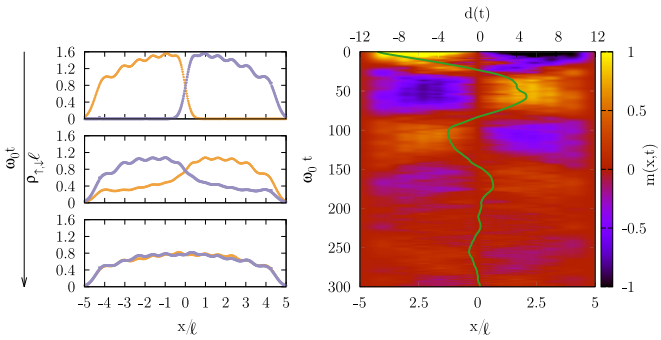

FIG. 1. Left panel: Spin up $\rho_\uparrow$ in orange (light gray) and down $\rho_\downarrow$ in violet (dark gray) spatial densities (in units of the inverse harmonic oscillator length ℓ^{-1}, with $\ell = \sqrt{\hbar/m\omega_0}$) as a function of position in the trap (in units of ℓ) at times $\omega_0 t = 0, 33, 200$ from top to bottom. The two initially separated clouds start oscillating in the trap and eventually fully mix, approaching to a zero-magnetization state. Right panel: Magnetization as a function of x (in units of ℓ) and t (in units of ω_0^{-1}) for $N = 12$ fermions. The green line corresponds to center of mass $d(t)$ of the magnetization.

system reads

$$H = \sum_{i=1}^{N}\left(\frac{p_i^2}{2m} + \frac{m\omega_0^2 x_i^2}{2}\right) + g\sum_{i\neq j}\delta(x_i - x_j), \tag{1}$$

where $N = N_\uparrow + N_\downarrow$ is the total number of particles and we take $N_\uparrow = N_\downarrow$, ω_0 is the frequency of the harmonic trap, and we model the interspecies interaction using a delta potential of strength g. Hamiltonian (1) is characterized by the symmetry under exchange of particles having the same spin. For $SU(2)$ fermions, the eigenstates can be classified by the irreducible representations of the permutation group (see, e.g., Ref. [20]).

We focus on the strongly repulsive limit $g \to \infty$: in this regime the model is exactly solvable [18] and the wave function is given by

$$\Psi = \sum_P \theta(x_{P(1)} < \cdots < x_{P(N)})\, a_P \Psi_A(x_1, \ldots, x_N), \tag{2}$$

where $\theta(x_1 < x_2 < x_3 < \ldots x_N)$ is the characteristic function of the coordinate sector $\{x_1 < x_2 < x_3 < \cdots < x_N\}$, a_P are phases depending on the spin ordering of the corresponding coordinate sector, and the summation is performed over all the possible permutations P of N elements. The function Ψ_A is the wave function of a N-particle noninteracting Fermi gas in the same external potential, i.e., the antisymmetric product of N eigenfunctions of the harmonic oscillator. Remarkably, in the $g \to \infty$ limit the spin and spatial ("charge") degrees of freedom are decoupled in the wave function.

We determine the phases a_p in Eq. (2) to first order in $1/g$ by mapping the Hamiltonian (1) into an effective spin chain:

$$H_s = \left(E_F - \sum_i^{N-1} J_i\right)\mathbb{1} + \sum_{i=1}^{N-1} J_i P_{i,i+1}, \tag{3}$$

where $P_{i,i+1}$ is the transposition operator on the chain of N sites and $E_F = N^2\hbar\omega_0/2$ is the Fermi energy. The coefficients J_i are site-dependent hopping parameters of the chain, carrying information on the external potential and on the atom-atom interaction of the original fermionic problem (see Supplemental Material [41]). The explicit expression reads [42]

$$J_i = \frac{1}{g}\int_{-\infty}^{\infty} dx_1 \ldots dx_N\, \delta(x_i - x_{i+1})\, \theta(x_1 < \cdots < x_N)\left|\frac{\partial \Psi_A}{\partial x_i}\right|^2. \tag{4}$$

We classify the basis vectors of the Hilbert space associated to (3) according to the spin ordering on the chain (the so-called snippet basis [19]). For example, for $N_\uparrow = N_\downarrow = 2$ the vector $|\uparrow\uparrow\downarrow\downarrow\rangle$ indicates that all the spins $\uparrow$ are placed in the left half of the chain. Therefore, the dimension of the Hilbert space is $s = \frac{N!}{N_\uparrow! N_\downarrow!}$. The diagonalization of Eq. (3) allows us to calculate the a_P and thus several observables such as the spin densities $\rho_{\uparrow,\downarrow}(x,t)$. This allows us to study the dynamics of the trapped system with an arbitrary initial state.

In this Letter we follow the fermion dynamics starting from the initially strongly out-of-equilibrium state $|\chi(t = 0)\rangle = |\uparrow\uparrow\uparrow \ldots \downarrow\downarrow\downarrow\rangle$, as in Ref. [11], where the spins up and down are separated in the two opposite sides of the trap. Since the harmonic trap is unchanged, the spatial part of the wave function (2) is constant during the motion, hence J_i are constant in time. The time evolution involves only the spin degrees of freedom and can be obtained using the effective spin chain Hamiltonian (3). Recalling that the spin operators are related to the permutation operator by the relation $P_{k,k+1} = \frac{1}{2}(\mathbb{1} + \sigma_k\sigma_{k+1})$, Hamiltonian (1) can be mapped to the one of an inhomogeneous isotropic Heisenberg model $H_H = \sum_{j=1}^{N-1} J_j \vec{\sigma}_j \cdot \vec{\sigma}_{j+1}$, but *in particle space*, i.e., each lattice site is associated to a particle index. The equation of motion for the spin operator $\vec{S}_j = \frac{1}{2}(\sigma_j^x, \sigma_j^y, \sigma_j^z)$ for the jth particle reads

$$\frac{dS_j^\mu}{dt} = i\left[H_s, S_j^\mu\right] = (\vec{\tau}_j \times \vec{S}_j)^\mu, \tag{5}$$

where $\mu = x, y, z$ and $\vec{\tau}_j = J_{j-1}\vec{\sigma}_{j-1} + J_j\vec{\sigma}_{j+1}$ is the torque acting on a fixed particle due to the coupling with the neighboring ones [41]. As a result of Eq. (5) we conclude that in our case the spin dynamics is entirely due to spin torque [41].

The experimentally accessible component of such spin vector is S_j^z, associated to the local magnetization

$$m(x,t) = \sum_{j=1}^{N} m_j(t)\rho_j(x), \tag{6}$$

where $\rho_j(x)$ is the spatial density of the jth particle in the trap [26,41], $m_j(t) = \langle\chi(t)|S_j^z|\chi(t)\rangle$, and $|\chi(t)\rangle = e^{-iH_s t}|\chi(0)\rangle$ is the time-evolved spin state, obtained from the diagonalization of H_s by exploiting all its symmetries. The magnetization is experimentally accessible by recording the population imbalance among $\uparrow$ and $\downarrow$ fermions, $m(x,t) = \rho_\uparrow(x,t) - \rho_\downarrow(x,t)$.

Another important observable for the dynamics is the spin current density

$$j(x,t) = \frac{1}{2}\sum_{j=1}^{N-1} j_j(t)[\rho_j(x) + \rho_{j+1}(x)], \tag{7}$$

where $j_j(t)$ are obtained from the z component of Eq. (5), $j_j(t) = J_j(\sigma_j^x\sigma_{j+1}^y - \sigma_j^y\sigma_{j+1}^x)$. We detail in the following the spin-mixing dynamics in the various relevant time regimes.

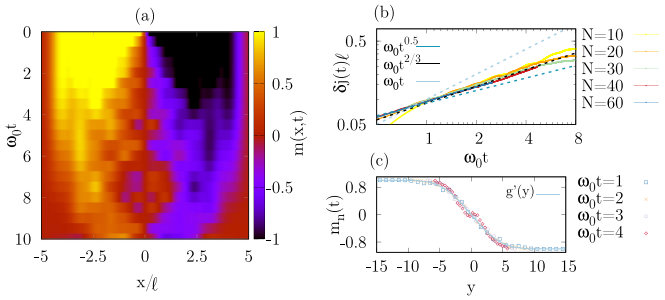

FIG. 2. (a) Early-time magnetization dynamics $m(x,t)$ from exact solution for $N = 12$ as a function of space (x in units of ℓ) and time t (in units of ω_0^{-1}). (b) Integrated current $\delta j(t)$ in units of ℓ^{-1} from the density-matrix renormalization group, as a function of time t (in units of ω_0^{-1}) evaluated in the center of the trap $x = 0$ (solid lines), together with ballistic $\delta j \sim t$, KPZ $\delta j \sim t^{2/3}$, and diffusive behavior $\delta j \sim t^{1/2}$ (dashed straight lines). A larger number of particles are associated with increasingly darker colors. (c) KPZ scaling of the magnetization $m_n(t)$, shown as a function of $y = n/(\omega_0 t)^{2/3}$. We show the comparison with the derivative of the suitably renormalized 1D KPZ scaling function $g(y)$ [45].

Systems up to $N = 12$ particles have been analyzed using exact diagonalization, while we used truncated Taylor series approximation of the time evolution operator [43] and the time-dependent density-matrix renormalization group (tDMRG) [44] to study larger systems.

III. SHORT TIMES

The short-time dynamics, before the first spin oscillation, is shown in Fig. 2. We show the magnetization as a function of space and time, showing that the initially sharp magnetization interface spreads with time, until it starts feeling the effect of the confining potential. To identify the nature of the magnetization spreading, it is useful to study the time-integrated spin current density as in Ref. [28], $\delta j(t) = \int_0^t dt'\, j(0,t')$, where $j(x,t)$ is defined in Eq. (7) and it is calculated at the center of the trap. We see that the integrated spin current displays a superdiffusive behavior $\delta j(t) \sim t^\eta$, with power-law exponent $\eta \sim 0.638(1)$. This is compatible with the value $\eta = 2/3$ predicted for the homogeneous spin chain and clearly not ballistic or diffusive. Remarkably, low-energy dynamics described by Luttinger liquid predicts ballistic behavior [1]: the deviation from this prediction discloses the marked out-of-equilibrium features of the physical system that are described in an exact way by our model. Using DMRG calculations we have checked that the KPZ region persists for larger numbers of particles (see Fig. 2) The deviation at later times from KPZ behavior is due to onset of the oscillatory dynamics associated to the presence of the external trap. Within the KPZ region, we find that the magnetization profiles collapse onto each other if plotted as a function of $x_n/(\omega_0 t)^{1/z}$, $z = 3/2$ being the KPZ value for the dynamical critical exponent.

IV. INTERMEDIATE TIMES

We next focus on the intermediate-time regime, when the particles undergo large-amplitude spin-dipole oscillations in the trap. We follow the center-of-mass oscillations of the magnetization:

$$d(t) = \frac{1}{N}\int_{-\infty}^{\infty} dx\, x\, m(x,t). \tag{8}$$

The time evolution of $d(t)$ is shown in Fig. 3(a) for various values of the number of particles. We observe damped oscillations tending to a plateau corresponding to zero magnetization. At later times (not shown in the figure), the dynamics undergoes several partial revivals, as expected since we describe a closed quantum system. Quite remarkably, we find that the various curves for different particle numbers collapse one to another if we scale the time axis by a factor N^α with $\alpha = 0.25$. Using DMRG simulations up to $N = 60$ particles [41], we have tested that the scaling is robust at increasing particle numbers. The magnetization oscillations are well approximated by a damped harmonic oscillator $F(t) = f_0 e^{-\gamma t}\cos(\Omega t)$ [see Fig. 3(b)]. This allows us to obtain the oscillation frequency Ω for the various N values. We find that the damping rate γ does not depend on the number of particles. Combining the two values, we obtain the spin drag rate as $\Gamma_{\rm SD} = \Omega^2/\gamma$ [3,4,11,46].

We also perform a spectral analysis of $d(t)$ by introducing the spectral function $A(\omega) = \int_0^\infty dt\; d(t) e^{i\omega t}$. In Fig. 3(c) we show $|A(\omega)|$ and the Fourier transform of the fitted signal $\tilde{F}(\omega) = \int_0^\infty dt\; F(t) e^{i\omega t}$ as a function of the rescaled frequencies. The spectral function shows two main peaks centered around $\pm\Omega_{\rm univ}$. Several excitation frequencies contribute to the overall shape and the linewidth of $\tilde{F}(\omega)$ [41]. To estimate the scaling exponent α we evaluate the position $P_N(\alpha) = \omega_P N^\alpha$ of the maximum of $\tilde{F}(\omega N^\alpha)$ at positive frequencies, such that $\tilde{F}(\omega_P N^\alpha) = \max_{\omega>0}\tilde{F}(\omega N^\alpha)$, as a function of a scaling exponent α. As we show in Fig. 3(d), the universal scaling is reached for $\alpha = 0.25$.

The universal scaling observed in Fig. 3 allows us to estimate the spin-dipole oscillation frequency at larger N as $\Omega_N \simeq \Omega_{\rm univ}/N^{1/4}$, with $\Omega_{\rm univ} \simeq 0.19\,\omega_0$. Correspondingly, we find that the spin drag scales as $\Gamma_{\rm SD} = \Omega_{\rm univ}^2/(\gamma N^{1/2})$, hence vanishing at large particle numbers, as also predicted in Ref. [1] for low-energy excitations of the spectrum.

V. LONG TIMES

Finally, we study the long-time regime at which the damped dynamics becomes dominant and the system approaches to a zero-magnetization state. Since the Hamiltonian (1) is not integrable at finite interaction strength, we expect some traces of chaoticity to emerge during the dynamics [40,47,48]. In this case the system thermalizes to a state described by the diagonal ensemble, coinciding in our case with the microcanonical ensemble [49]. We verify this by calculating the distance $R(t) = \int dx\, |\rho_\uparrow(x,t) - \rho_{\uparrow,\rm MC}(x)|^2$ between the spin-up density and its value in the microcanonical ensemble $\rho_{\uparrow,\rm MC}(x)$. The results are presented in Fig. 4(a). At times corresponding to the zero-magnetization plateau in Fig. 4, $R(t)$ vanishes and the spin density approaches to the steady-state value. At later times, revivals occur and the system deviates from this configuration.

To further provide evidence for chaotic behavior, we analyze the level-spacing distribution $W(\Delta\epsilon)$ [50–52], constructed using the unfolded dimensionless energy levels

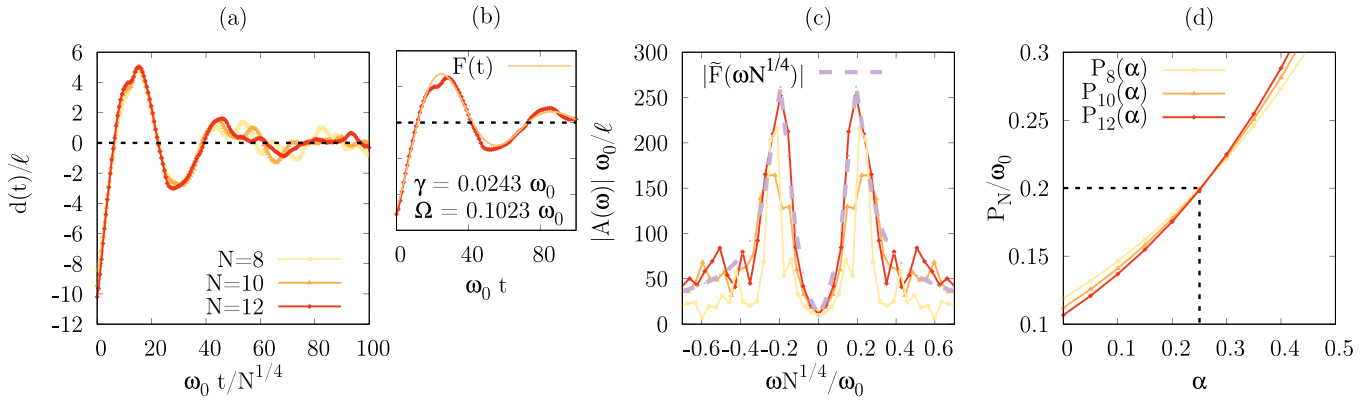

FIG. 3. (a) Center of mass of the magnetization $d(t)$, in units of ℓ, as a function of time, in units of ω_0^{-1}, and scaled by a factor $N^{1/4}$ to evidence the universal behavior of the oscillations. (b) $d(t)$ for $N = 12$ fitted with a damped harmonic oscillator $F(t) = f_0 e^{-\gamma t}\cos(\Omega t)$. (c) Modulus of $A(\omega)$, in units of ℓ/ω_0, for different numbers of particles as a function of the universal frequencies $\omega N^{1/4}/\omega_0$, compared to the modulus of the Fourier transform $\tilde{F}(\omega)$ of the fit $F(t)$ (dotted violet line). Color codes are the same as in panel (a). (d) Position $P_N(\alpha)$ of the peaks of $\tilde{F}(\omega N^{\alpha})$, in units of ω_0, as a function of the scaling parameter α.

[48,53–55]. The spectrum of an integrable system follows a Poissonian distribution $W_P(\Delta\epsilon) = e^{-\Delta\epsilon}$, while a chaotic system is described by a Wigner-Dyson one $W_{\mathrm{WD}}(\Delta\epsilon) = \frac{\pi}{2}\Delta\epsilon\, e^{-\frac{\pi}{4}\Delta\epsilon^2}$. We interpolate between the two regimes, thus quantifying the level of chaoticity encoded in the spectrum, through the Brody distribution [56]:

$$W_B(\Delta\epsilon) = (\beta+1)b\Delta\epsilon^{\beta} e^{-b\Delta\epsilon^{\beta+1}}, \tag{9}$$

where $b = \{\Gamma[(\beta+2)/(\beta+1)]\}^{\beta+1}$ and Γ is the Euler Gamma function. The Brody distribution reduces to the Poisson or Wigner-Dyson ones for $\beta = 0$ or 1, respectively.

To obtain the level-spacing distribution it is important to take into account the symmetries of the system [57], which in our case are the spatial parity and the symmetry under particle exchange. Our choice of basis vectors allows us to readily check the parity of the eigenstates. In order to identify the symmetry under particle exchange associated to a given Young tableau, we diagonalize the Heisenberg Hamiltonian in the basis of the permutational symmetry [20,58]. We then partition the energy levels according to the quantum numbers of the corresponding eigenstates. In the inset in Fig. 4(b) we show the distribution of all the unfolded level spacings, irrespective of the symmetry constraints. In this case the chaoticity is hidden and the distribution is Poissonian. The level-spacing distribution of the largest subspace at fixed symmetry is shown in the main panel of Fig. 4(b). We find that the level-spacing distribution is well described by the Brody distribution with parameter $\beta = 0.22$. This shows that large interactions destroy only partially the integrability of the infinite-repulsion model. A moderately chaotic behavior also emerges from the study of the localization properties of the eigenstates of the Hamiltonian (1) [41]. Such intermediate regime is typical of integrable systems subjected to small perturbations [48,51,59].

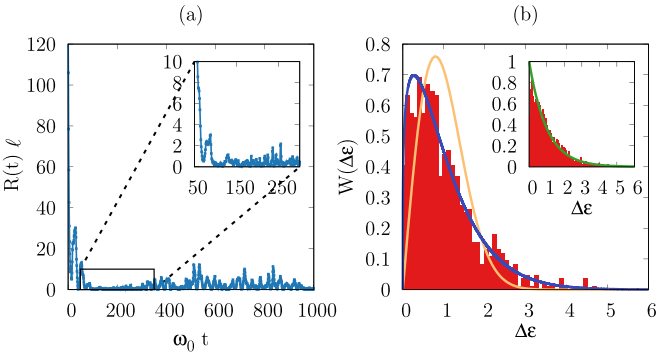

FIG. 4. (a) Distance $R(t)$ (in units of ℓ^{-1}) as a function of time (in units of ω_0^{-1}). The inset shows a zoom of the area indicated by the rectangle. (b) Level-spacing distribution $W(\Delta\epsilon)$ for the unfolded spectrum in a sector at fixed symmetry. The orange and the blue curves show, respectively, the Wigner-Dyson $W_{WD}(\Delta\epsilon)$ and the Brody distribution $W_B(\Delta\epsilon)$ with $\beta = 0.22$. The inset shows the level-spacing distribution of the whole unfolded spectrum and the Poisson distribution $W_P(\Delta\epsilon)$ (green line). In all the panels, $N = 14$.

VI. CONCLUSIONS

We have studied the strongly out-of-equilibrium spin-mixing dynamics of repulsive 1D fermions under harmonic confinement, starting from an initial spatially separated spin configuration. Thanks to the mapping to an inhomogeneous Heisenberg model on an effective lattice in particle space, we have followed the real-space magnetization dynamics until very long times. At short times, specific to one-dimensional systems and different from the three-dimensional strongly interacting Fermi gas, we observe superdiffusive behavior of the magnetization profile in time. The system here considered is weakly not integrable and hence equivalent to the case where KPZ universality was reported in the short-time dynamics [35,60,61]. Our observations call for the exploration of the universal properties of the corresponding spin model. At intermediate times, we have obtained damped spin-dipole oscillations characterized by a universal scaling of the oscillation time with $N^{1/4}$, thus predicting a slowdown of the oscillation and decrease of spin drag at large particle numbers. At long times, we find that the system

thermalizes to a diagonal ensemble state thanks to its moderately chaotic behavior. All our conclusions hold exactly for strongly repulsive interactions to order $1/g$. A study of itinerant fermions at arbitrary interactions and long times remains an open challenge. Our results show that harmonically trapped strongly interacting fermions are a promising platform for exploring the many facets of the nonequilibrium quantum dynamics.

ACKNOWLEDGMENTS

We would like to thank Maxim Olshanii and Giacomo Roati for stimulating discussions, Pierre Nataf for his assistance in the early stages of this work, and Piero Naldesi for his significant help with DMRG calculations. We acknowledge funding from Grant No. ANR-21-CE47-0009 in the Quantum-SOPHA project.

[1] M. Polini and G. Vignale, Phys. Rev. Lett. **98**, 266403 (2007).
[2] D. Ralph and M. Stiles, J. Magn. Magn. Mater. **320**, 1190 (2008).
[3] I. D'Amico and G. Vignale, Phys. Rev. B **62**, 4853 (2000).
[4] I. D'Amico and G. Vignale, Phys. Rev. B **65**, 085109 (2002).
[5] T. Enss and R. Haussmann, Phys. Rev. Lett. **109**, 195303 (2012).
[6] F. Carlini and S. Stringari, Phys. Rev. A **104**, 023301 (2021).
[7] G. Valtolina, F. Scazza, A. Amico, A. Burchianti, A. Recati, T. Enss, M. Inguscio, M. Zaccanti, and G. Roati, Nat. Phys. **13**, 704 (2017).
[8] A. G. Volosniev, D. Petrosyan, M. Valiente, D. V. Fedorov, A. S. Jensen, and N. T. Zinner, Phys. Rev. A **91**, 023620 (2015).
[9] R. E. Barfknecht, A. Foerster, and N. T. Zinner, Sci. Rep. **9**, 15994 (2019).
[10] M. Mestyán, B. Bertini, L. Piroli, and P. Calabrese, Phys. Rev. B **99**, 014305 (2019).
[11] A. Sommer, M. Ku, G. Roati, and M. W. Zwierlein, Nature (London) **472**, 201 (2011).
[12] M. Gaudin, Phys. Lett. A **24**, 55 (1967).
[13] C. N. Yang, Phys. Rev. Lett. **19**, 1312 (1967).
[14] A. Syrwid, M. Łebek, P. T. Grochowski, and K. Rzążewski, Phys. Rev. A **105**, 013314 (2022).
[15] G. Koutentakis, S. Mistakidis, and P. Schmelcher, New J. Phys. **21**, 053005 (2019).
[16] T. Kinoshita, T. Wenger, and D. S. Weiss, Nature (London) **440**, 900 (2006).
[17] N. L. Harshman, M. Olshanii, A. S. Dehkharghani, A. G. Volosniev, S. G. Jackson, and N. T. Zinner, Phys. Rev. X **7**, 041001 (2017).
[18] A. Volosniev, D. V. Fedorov, A. S. Jensen, M. Valiente, and N. T. Zinner, Nat. Commun. **5**, 5300 (2014).
[19] F. Deuretzbacher, K. Fredenhagen, D. Becker, K. Bongs, K. Sengstock, and D. Pfannkuche, Phys. Rev. Lett. **100**, 160405 (2008).
[20] J. Decamp, P. Armagnat, B. Fang, M. Albert, A. Minguzzi, and P. Vignolo, New J. Phys. **18**, 055011 (2016).
[21] B. Fang, P. Vignolo, M. Gattobigio, C. Miniatura, and A. Minguzzi, Phys. Rev. A **84**, 023626 (2011).
[22] S. Murmann, F. Deuretzbacher, G. Zürn, J. Bjerlin, S. M. Reimann, L. Santos, T. Lompe, and S. Jochim, Phys. Rev. Lett. **115**, 215301 (2015).
[23] M. Boll, T. A. Hilker, G. Salomon, A. Omran, J. Nespolo, L. Pollet, I. Bloch, and C. Gross, Science **353**, 1257 (2016).
[24] B. Sutherland, *Beautiful Models: 70 Years of Exactly Solved Quantum Many-Body Problems* (World Scientific, Singapore, 2004).
[25] F. Franchini, *An Introduction to Integrable Techniques for One-Dimensional Quantum Systems* (Springer, New York, 2017).
[26] F. Deuretzbacher, D. Becker, J. Bjerlin, S. M. Reimann, and L. Santos, Phys. Rev. A **90**, 013611 (2014).
[27] F. Deuretzbacher, D. Becker, and L. Santos, Phys. Rev. A **94**, 023606 (2016).
[28] M. Ljubotina, M. Žnidarič, and T. Prosen, Nat. Commun. **8**, 16117 (2017).
[29] D. Gobert, C. Kollath, U. Schollwöck, and G. Schütz, Phys. Rev. E **71**, 036102 (2005).
[30] E. Ilievski, J. De Nardis, M. Medenjak, and T. c. v. Prosen, Phys. Rev. Lett. **121**, 230602 (2018).
[31] J. De Nardis, M. Medenjak, C. Karrasch, and E. Ilievski, Phys. Rev. Lett. **123**, 186601 (2019).
[32] M. Ljubotina, M. Žnidarič, and T. c. v. Prosen, Phys. Rev. Lett. **122**, 210602 (2019).
[33] S. Gopalakrishnan and R. Vasseur, Phys. Rev. Lett. **122**, 127202 (2019).
[34] M. Dupont and J. E. Moore, Phys. Rev. B **101**, 121106(R) (2020).
[35] A. Bastianello, B. Bertini, B. Doyon, and R. Vasseur, J. Stat. Mech.: Theory Exp. (2022) 014001.
[36] V. B. Bulchandani, Phys. Rev. B **101**, 041411(R) (2020).
[37] M. Iversen, R. E. Barfknecht, A. Foerster, and N. T. Zinner, J. Phys. B **53**, 155301 (2020).
[38] D. Wei, A. Rubio-Abadal, B. Ye, F. Machado, J. Kemp, K. Srakaew, S. Hollerith, J. Rui, S. Gopalakrishnan, N. Y. Yao, I. Bloch, and J. Zeiher, arXiv:2107.00038.
[39] A. Scheie, N. Sherman, M. Dupont, S. Nagler, M. Stone, G. Granroth, J. Moore, and D. Tennant, Nat. Phys. **17**, 726 (2021).
[40] M. Rigol, V. Dunjko, and M. Olshanii, Nature (London) **452**, 854 (2008).
[41] See Supplemental Material at http://link.aps.org/supplemental/10.1103/PhysRevA.105.L051303 for the derivation and further details.
[42] To compute the hopping coefficients J_i we used the open source code CONAN [62].
[43] A. H. Al-Mohy and N. J. Higham, SIAM J. Sci. Comput. **33**, 488 (2011).
[44] S. Peotta, D. Rossini, P. Silvi, G. Vignale, R. Fazio, and M. Polini, Phys. Rev. Lett. **108**, 245302 (2012).
[45] M. Prähofer and H. Spohn, https://www-m5.ma.tum.de/KPZ.
[46] Here we assume that the spin drag is constant over the time of the damped oscillations. The study of a larger system would be required to test this hypothesis.
[47] M. Ueda, Nat. Rev. Phys. **2**, 669 (2020).
[48] L. F. Santos, F. Borgonovi, and F. M. Izrailev, Phys. Rev. E **85**, 036209 (2012).

[49] L. D'Alessio, Y. Kafri, A. Polkovnikov, and M. Rigol, Adv. Phys. **65**, 239 (2016).
[50] T. Guhr, A. Müller-Groeling, and H. A. Weidenmüller, Phys. Rep. **299**, 189 (1998).
[51] L. F. Santos and M. Rigol, Phys. Rev. E **81**, 036206 (2010).
[52] F. Borgonovi, F. Izrailev, L. Santos, and V. Zelevinsky, Phys. Rep. **626**, 1 (2016).
[53] A. Gubin and L. F. Santos, Am. J. Phys. **80**, 246 (2012).
[54] Unfolding is obtained by normalizing the energy levels such that the mean level spacing is equal to 1 everywhere in the spectrum.
[55] L. F. Santos, J. Math. Phys. **50**, 095211 (2009).
[56] T. A. Brody, J. Flores, J. B. French, P. A. Mello, A. Pandey, and S. S. M. Wong, Rev. Mod. Phys. **53**, 385 (1981).
[57] C. Stone, Y. A. E. Aoud, V. A. Yurovsky, and M. Olshanii, New J. Phys. **12**, 055022 (2010).
[58] P. Nataf and F. Mila, Phys. Rev. Lett. **113**, 127204 (2014).
[59] L. F. Santos, J. Phys. A: Math. Gen. **37**, 4723 (2004).
[60] J. De Nardis, S. Gopalakrishnan, R. Vasseur, and B. Ware, Phys. Rev. Lett. **127**, 057201 (2021).
[61] J. De Nardis, S. Gopalakrishnan, R. Vasseur, and B. Ware, arXiv:2109.13251.
[62] N. Loft, L. Kristensen, A. Thomsen, A. Volosniev, and N. Zinner, Comput. Phys. Commun. **209**, 171 (2016).